Available online at www.sciencedirect.com
ScienceDirect
International Journal of Heat and Mass Transfer 51 (2008) 1888–1906
International Journal of HEAT and MASS TRANSFER
www.elsevier.com/locate/ijhmt

A numerical study of natural convection in a square enclosure with a circular cylinder at different vertical locations

B.S. Kim [a], D.S. Lee [a], M.Y. Ha [a,*], H.S. Yoon [b]

[a] Department of Mechanical Engineering, Pusan National University, Jang Jeon 2-Dong, Geum Jeong Gu, Busan 609-735, Republic of Korea
[b] Advanced Ship Engineering Research Center, Pusan National University, Jang Jeon 2-Dong, Geum Jeong Gu, Busan 609-735, Republic of Korea

Received 2 March 2007; received in revised form 19 June 2007
Available online 27 August 2007

Abstract

Numerical calculations are carried out for natural convection induced by a temperature difference between a cold outer square enclosure and a hot inner circular cylinder. A two-dimensional solution for unsteady natural convection is obtained, using the immersed boundary method (IBM) to model an inner circular cylinder based on the finite volume method for different Rayleigh numbers varying over the range of 10^3–10^6. The study goes further to investigate the effect of the inner cylinder location on the heat transfer and fluid flow. The location of the inner circular cylinder is changed vertically along the center-line of square enclosure. The number, size and formation of the cell strongly depend on the Rayleigh number and the position of the inner circular cylinder. The changes in heat transfer quantities have also been presented.

1. Introduction

Natural convection in an enclosure is relevant to many industrial and environmental applications such as heat exchangers, nuclear and chemical reactors, cooling of electronic equipment, and stratified atmospheric boundary layers. In engineering applications, the geometries that arise, however, are more complicated than a simple enclosure filled with a convective fluid. The geometric configuration of interest is with the presence of bodies embedded within the enclosure. (Lacroix [1]; Ghaddar and Thiele [2]; Saha [3]; Ding et al. [4]).

Many investigations have dealt with the presence of a body with various thermal conditions on natural convection within a square enclosure with either a horizontally (Ha et al. [5,6]; Lee et al. [7–9]) or vertically (Hyun and Lee [10]; Misra and Sarkar [11]; Wright et al. [12]; McBain [13]; Jami et al. [14]; Ha and Jung [15]) imposed temperature difference or heat flux.

The similarly relevant case of natural convection that occurs from a heated body placed concentrically or eccentrically inside a cooled enclosure has received much less attention.

Asan [16] numerically studied two-dimensional natural convection in an annulus between two isothermal concentric square ducts and obtained solutions up to a Rayleigh number of 10^6. The results showed that dimension ratio and Rayleigh number have a profound influence on the temperature and flow field.

Kumar De and Dalal [17] considered the problem of natural convection around a square, horizontal, heated cylinder placed inside an enclosure in the range of $10^3 \leqslant Ra \leqslant 10^6$. Effects of the enclosure geometry have been assessed using three different aspect ratios placing the square cylinder at different heights from the bottom. As a result, it was found that the uniform wall temperature heating is quantitatively different from the uniform wall heat flux heating. The flow pattern and thermal stratification were modified, if the aspect ratio was varied. Overall heat transfer also changes as a function of aspect ratio.

Ghaddar [18] reported the numerical results of natural convection from a uniformly heated horizontal cylinder

* Corresponding author. Tel.: +82 51 510 2440; fax: +82 51 581 3718.
E-mail address: myha@pusan.ac.kr (M.Y. Ha).

0017-9310/$ - see front matter © 2007 Elsevier Ltd. All rights reserved.
doi:10.1016/j.ijheatmasstransfer.2007.06.033

Nomenclature

f_i	momentum forcing
g	gravity
h	heat source or sink
L	wall length
L_c	length around circular cylinder
n	normal direction to the wall
Nu	local Nusselt number
$\overline{Nu}_B$	surface-averaged Nusselt number at the bottom wall of square enclosure
$\overline{Nu}_c$	surface-averaged Nusselt number of circular cylinder
$\overline{Nu}_{en}$	surface-averaged Nusselt number of square enclosure
$\overline{Nu}_S$	surface-averaged Nusselt number at the side wall of square enclosure
$\overline{Nu}_T$	surface-averaged Nusselt number at the top wall of square enclosure
P	pressure
Pr	Prandtl number
q	mass source or sink
r	radius of circular cylinder
Ra	Rayleigh number
S	distance along the square enclosure
t	time
T	dimensional temperature
T_h	high temperature
T_c	low temperature
u, v	velocity components in x and y directions
W	surface area of walls
x, y	Cartesian coordinates

Greek symbols

α	thermal diffusivity
β	thermal expansion coefficient
δ	distance from center of square cylinder to circular cylinder center
δ_{i2}	kronecker delta
ρ	density
ν	kinematic viscosity
φ	angle of circular cylinder
θ	dimensionless temperature

Sub/Superscripts

*	dimensionless value
–	surface-averaged quantity

placed in a large air-filled rectangular enclosure. He observed that flow and the thermal behaviors depend on heat fluxes imposed on the inner cylinder within the isothermal enclosure. He also obtained a correlation of the average Nusselt number as a function of Rayleigh number.

Cesini et al. [19] performed the numerical and experimental analysis of natural convection from a horizontal cylinder enclosed in a rectangular cavity. The influence of the cavity aspect ratio and the Rayleigh number on the distribution of temperature and Nusselt number was investigated. As a result, the average heat transfer coefficients increases with increasing Rayleigh number.

Moukalled and Acharya [20] and Shu and Zhu [21] studied the change of the thermo-flow field between the low temperature outer square enclosure and high temperature inner circular cylinder according to the radius of the inner circular cylinder. Moukalled and Acharya [20] considered three different aspect ratios, r/L of the cylinder radius, r to the enclosure height, L in the range of $10^4 \leqslant Ra \leqslant 10^7$. They showed that, at a constant enclosure aspect ratio, the total heat transfer increases with increasing Rayleigh number. When the Rayleigh number is constant, the convection contribution to the total heat transfer decreases with an increasing aspect ratio value. Shu and Zhu [21] obtained the numerical results for Rayleigh numbers ranging from 10^4 to 10^6 and aspect ratios between 1.67 and 5.0. It was found that both the aspect ratio and the Rayleigh number are critical to the patterns of flow and thermal fields. Also, they suggested that a critical aspect ratio may exist at high Rayleigh numbers to distinguish the flow and thermal patterns.

Shu et al. [22] numerically studied natural convection between an outer square enclosure and an inner circular cylinder according to the eccentricity and angular position of the inner circular cylinder at a Rayleigh number of 3×10^5. Natural convection between arbitrary eccentric cylinders for $Ra = 3 \times 10^5$ and a specified aspect ratio of r/L was systematically analyzed, including the effects of an outer cylinder position on the average Nusselt number, flow and thermal fields. It was found that the global circulation, flow separation and the top space between the square outer enclosure and the circular inner cylinder have significant effects on the plume inclination.

However, there is little information about natural convection processes when a heated circular cylinder exists within a cooled square enclosure and the location of the inner heated circular cylinder is changed along the vertical centerline of the square enclosure. In this situation, the flow and heat transfer in the enclosure are largely affected by the location of the inner circular cylinder for different Rayleigh numbers. The purpose of the present study is to examine how the position of the inner circular cylinder relative to the outer square cylinder affects the natural convection phenomena for different Rayleigh numbers when a hot inner circular cylinder is located at different positions along the vertical centerline of the outer square cylinder.

2. Numerical methodology

A schematic of the system considered in the present study is shown in Fig. 1. The system consists of a square enclosure with sides of length L, within which a circular cylinder with a radius $R(=0.2\,L)$ is located and moves along the vertical centerline in the range from $-0.25\,L$ to $0.25\,L$. The walls of the square enclosure was kept at a constant low temperature of T_c, whereas the cylinder was kept at a constant high temperature of T_h. In this study, we assume that the radiation effects are negligible. The fluid properties are also assumed to be constant, except for the density in the buoyancy term, which follows the Boussinesq approximation. The gravitational acceleration acts in the negative y-direction. The immersed boundary method is used to handle the inner circular cylinder, which is located at different positions along the vertical direction, in Cartesian coordinates. Therefore, the governing equations describing unsteady incompressible viscous flow and the thermal fields in the present study are the continuity, momentum and energy equations in their non-dimensional forms defined as

$$\frac{\partial u_i}{\partial x_i} - q = 0 \tag{1}$$

$$\frac{\partial u_i}{\partial t} + u_j\frac{\partial u_i}{\partial x_j} = -\frac{\partial P}{\partial x_i} + Pr\frac{\partial^2 u_i}{\partial x_j \partial x_j} + RaPr\theta\delta_{i2} + f_i \tag{2}$$

$$\frac{\partial \theta}{\partial t} + u_j\frac{\partial \theta}{\partial x_j} = \frac{\partial^2 \theta}{\partial x_j \partial x_j} + h \tag{3}$$

The dimensionless variables in the above equations are defined as

$$t = \frac{t^*\alpha}{L^2}, \quad x_i = \frac{x_i^*}{L}, \quad u_i = \frac{u_i^* L}{\alpha}, \quad P = \frac{P^* L^2}{\rho\alpha^2}, \quad \theta = \frac{T - T_c}{T_h - T_c} \tag{4}$$

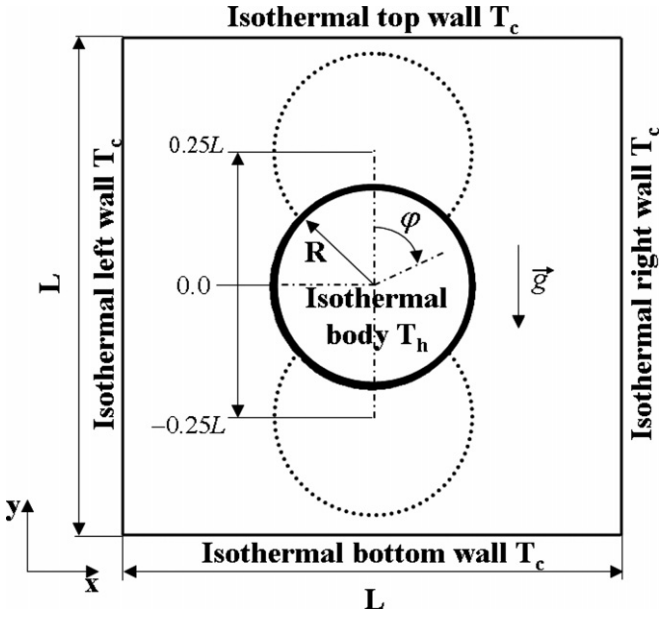

Fig. 1. Computational domain and coordinate system along with boundary conditions.

in the above equations, ρ, T and α represent the density, dimensional temperature and thermal diffusivity. The superscript * in Eq. (4) represents the dimensional variables. u_i, p, t, x_i and θ are the non-dimensional velocity, pressure, time and temperature. The above non-dimensionalization results in two dimensionless parameters: $Pr = \frac{\nu}{\alpha}$ and $Ra = \frac{g\beta L^3(T_h - T_c)}{\nu\alpha}$ where ν, g and β are the kinematic viscosity, gravitational acceleration and volume expansion coefficient. In the simulations to be reported here the Prandtl number, Pr, and $r(=R/L)$ have been taken to be 0.7 corresponding to that of air and 0.2, respectively. The Rayleigh number, Ra, varies in the range of 10^3–10^6. The dimensionless vertical distance δ, which represents the position of the inner cylinder along the vertical centerline, varies in the range of −0.25–0.25.

The mass source/sink q in Eq. (1) and momentum forcing f_i in Eq. (2) are applied on the body surface or inside the body to satisfy the no-slip condition and mass conservation in the cell containing the immersed boundary. In Eq. (3), the heat source/sink h is applied to satisfy the iso-thermal boundary condition on the immersed boundary.

A two-step time-split scheme was used to advance the flow field. This scheme was based on the previous works of Kim and Moin [23] and Zang et al. [24]. First the velocity is advanced from time level 'n' to an intermediate level '$*$' by solving the advection-diffusion equation without the pressure term. In the advection-diffusion step, the nonlinear terms are treated explicitly using the third-order Adams–Bashforth scheme. The diffusion terms are treated implicitly using Crank–Nicolson scheme. Then the Poisson equation for pressure, which is derived by using mass conservation, is solved fully implicitly. Once the pressure is obtained, the final divergence-free velocity field at '$n+1$' is obtained with a pressure-correction step. The temperature field is advanced in a similar manner with the third-order Adams–Bashforth scheme for the advection term and the Crank–Nicolson scheme for the diffusion term.

The central difference scheme with second-order accuracy based on the finite volume method is used for the spatial discretization. Additionally, a second-order linear or bilinear interpolation scheme is applied to satisfy the no-slip and isothermal conditions on the immersed boundary. Further details of the immersed-boundary method are given in Kim et al. [25] and Kim and Choi [26].

For the velocity field, the no-slip and no-penetration boundary conditions are imposed on the walls. The hot and cold wall temperatures of $\theta = 0$ and 1 are imposed on the walls of the enclosure and the inner cylinder wall, respectively.

Once the velocity and temperature fields are obtained, the local, surface-averaged, time-averaged, and time-and-surface-averaged Nusselt numbers are defined as

$$Nu = \left.\frac{\partial\theta}{\partial n}\right|_{\text{wall}}, \quad \overline{Nu} = \frac{1}{W}\int_0^W Nu\ \mathrm{d}S \tag{5}$$

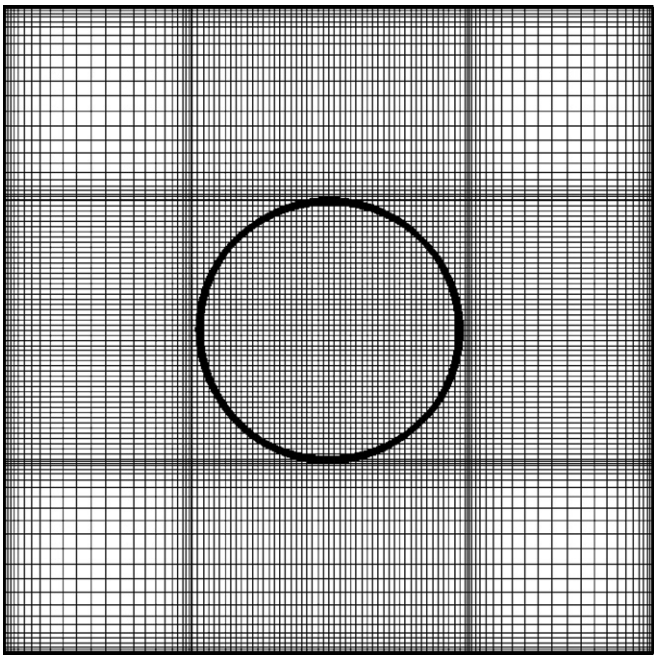

Fig. 2. A typical grid distribution for $\delta = 0$.

where n is the normal direction with respect to the walls, W is the surface area of walls.

Fig. 2 shows the computational geometry in the $x - y$ plane with a non-uniform grid distribution. A grid resolution of 201×201 along horizontal (x) and vertical (y) directions was employed in computations to be reported in this present study. The grids were nonuniformly distributed near the walls in order to account for the high gradients using the algebraic function. The denser grid lines were uniformly distributed within the cylinder. In order to consider the variation of δ, the number of grid points used in the y direction is tuned to maintain the dense resolution near the walls and within the inner cylinder. Grid independence of the solution has been tested with additional simulations on much finer grids up to $301(x) \times 301(y)$ points. The difference in the results of Nusselt number obtained using the coarse and fine grids was less than 0.3%.

For the purpose of code validation, the natural convection problem for a low temperature outer square enclosure and high temperature inner circular cylinder was tested. The calculated surface-averaged Nusselt numbers for the test case are compared with the benchmark values by Moukalled and Acharya [20] as shown in Table 1. The present surface-averaged Nusselt numbers are in good agreement with the values of Moukalled and Acharya [20].

Table 1
Comparison of present surface-averaged Nusselt number with those of previous numerical studies

Ra	Mean Nusselt number at hot wall		Difference (%)
	Present study	Moukalled and Acharya [16]	
10^4	3.414	3.331	−2.49
10^5	5.1385	5.08	−1.15
10^6	9.39	9.374	−0.17
10^7	15.665	15.79	0.79

3. Result and discussion

3.1. Flow and thermal fields when $\delta = 0$

Fig. 3 shows the isotherms and streamlines for different Rayleigh numbers when the inner circular cylinder is located at the center of the square enclosure corresponding to $\delta = 0$. For all Rayleigh numbers considered in this study, the flow and thermal fields eventually reach steady state with the symmetric shape about the vertical center line through the center of the inner circular cylinder. Thus, the present problem has a two-fold symmetry about the vertical center line at $x = 0$. In other words, the governing equations given in Eqs. (1)–(3) and the boundary conditions are invariant to the following transformation:

$$\text{Symmetry about } x = 0 : \{u, v, \theta, x, y\} \leftarrow \{-u, v, \theta, -x, y\} \tag{6}$$

The above two-fold symmetry of the problem can be seen in the steady flow and thermal fields. Thus the steady solutions of all the Rayleigh numbers considered in this study obey the underlying symmetries of the problem.

In general, the heated lighter fluid is lifted and moves upward along the hot surface of the inner cylinder and the vertical symmetry line until it encounters the cold top wall. Then the fluid becomes gradually colder and denser while it moves horizontally outward in contact with the cold top wall. Consequently, the cooled denser fluid descends along the cold side walls.

For $Ra = 10^3$, the heat transfer in the enclosure is mainly dominated by the conduction mode. The circulation of the flow shows two overall rotating symmetric eddies with two inner vortices respectively as shown in Fig. 3a for the streamlines. At $Ra = 10^4$, the patterns of the isotherms and streamlines are about the same as those for $Ra = 10^3$. However, a careful observation indicates that the thermal boundary layer on the bottom part of cylinder is thinner than that on the opposite side and the inner lower vortex slightly becomes smaller in size and weaker in strength compared with the upper one, because the effect of convection on heat transfer and flow increases with increasing the Rayleigh number.

As the Rayleigh number increases up to 10^5, the role of convection in heat transfer becomes more significant and consequently the thermal boundary layer on the surface of the inner cylinder becomes thinner. Also, a plume starts to appear on the top of the inner cylinder and as a result the isotherms move upward, giving rise to a stronger thermal gradient in the upper part of the enclosure and a much lower thermal gradient in the lower part. In consequence, the dominant flow is in the upper half of the enclosure, and correspondingly the core of the recirculating eddies is located only in the upper half. At this Rayleigh number,

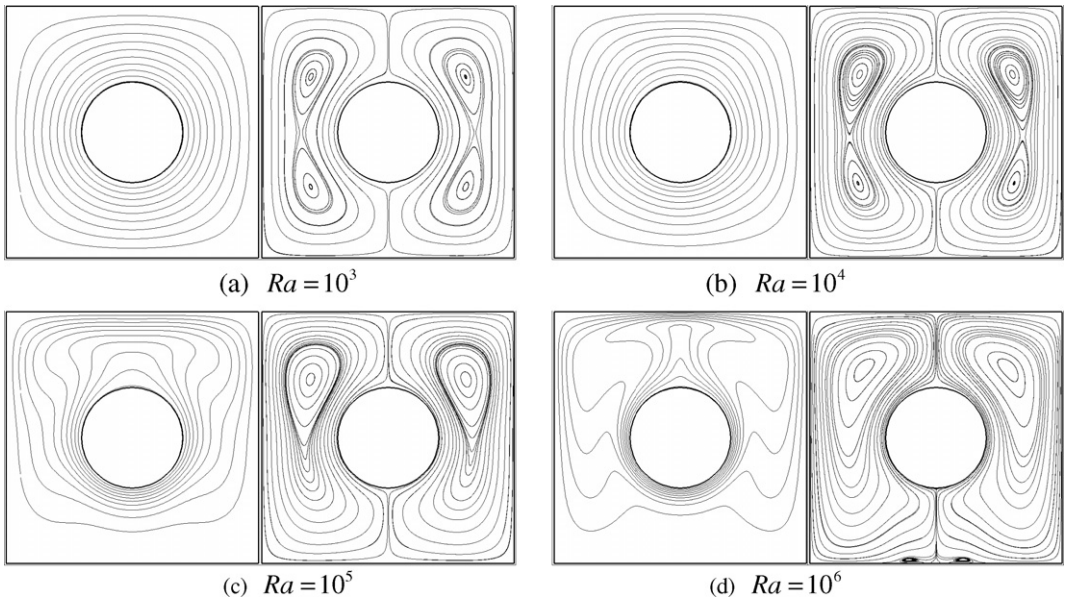

Fig. 3. Isothermals and streamlines at $\delta = 0.0$ for four different Rayleigh numbers of (a) 10^3, (b) 10^4, (c) 10^5 and (d) 10^6.

the flow filed undergoes a bifurcation where two inner vorticies merge. The flow at the bottom of the enclosure is very weak compared with that at the middle and top regions, which suggests stratification effects in the lower regions of the enclosure.

At $Ra = 10^6$, the heat transfer in the enclosure is mainly governed by the convection mode. Since the convection velocity significantly increases with increasing Rayleigh number, the boundary layer behavior can be clearly observed in regions of the lower part of cylinder and the upper part of the enclosure as shown in isotherms of Fig. 3d. The thermal boundary layer separates from the surface near the top of the cylinder and as a result a strong plume appears. As a result, the flow strongly impinges on the top of the enclosure, which also leads to form a thinner thermal boundary layer in this region and enhances the heat transfer. Tiny symmetric vortices appear in the vicinity of the bottom wall of the enclosure owing to the separation of the boundary layer by the strong convective flow.

3.2. Flow and temperature fields as a function of δ

3.2.1. $Ra = 10^3$

The dependence of the flow and thermal fields on δ can be observed in the plots of the isotherms and streamlines for the different δs at $Ra = 10^3$ shown in Fig. 4. Fig. 4a–e and f–j show the distribution of the isotherms and streamlines when the inner cylinder moves downward and upward at the same intervals of 0.05, respectively. Regardless of the δ variation, the solutions have a two-fold symmetry about the vertical center line at $x = 0$ corresponding to Eq. (6).

Because conduction is the dominant mode of heat transfer at this low Rayleigh number, the distribution of the flow and thermal fields in the left column of Fig. 4 for the negative δ value shows the symmetric shapes about the horizontal center line at $y = 0$, compared with that in the right column for the corresponding positive δ value.

When the cylinder moves downward decreasing δ, the size of the lower inner vortex is reduced gradually and the two inner vortices merge into a single vortex at $\delta = -0.15$ because the space between the inner cylinder and the bottom wall of the enclosure diminishes in size. On the other hand, the size of the upper inner vortex increases and its core moves toward the center of the enclosure because the enclosure can secure enough space to enlarge the circulation of the upper inner vortex. As δ becomes more negative, the isotherms become denser in between the lower part of the inner cylinder and the bottom wall, whereas they become coarser in the opposite region.

As the inner cylinder moves upward from the center of the enclosure, the thermal and flow fields in Fig. 4f–j show the symmetric shape about the horizontal center line at $y = 0$, compared with those as the inner cylinder moves downward as shown in Fig. 4a–e.

3.2.2. $Ra = 10^4$

Fig. 5 shows the distribution of isotherms and streamlines for different δs when $Ra = 10^4$. As Ra increases to 10^4, the effect of convection on heat transfer becomes larger than that at $Ra = 10^3$. Thus, the distribution of flow and thermal fields in the left column of Fig. 5 for the negative δ value shows the asymmetric shapes about the horizontal center line at $y = 0$, compared with that in the right column for the corresponding positive δ value. When the cylinder moves downward, the two inner vortices merge into a single vortex at $\delta = -0.1$, which is earlier than $\delta = -0.15$ at $Ra = 10^3$. As δ increases as a negative value, the isotherms are gradually distorted and the size of the thermal plumes formed on the top of the inner cylinder becomes larger.

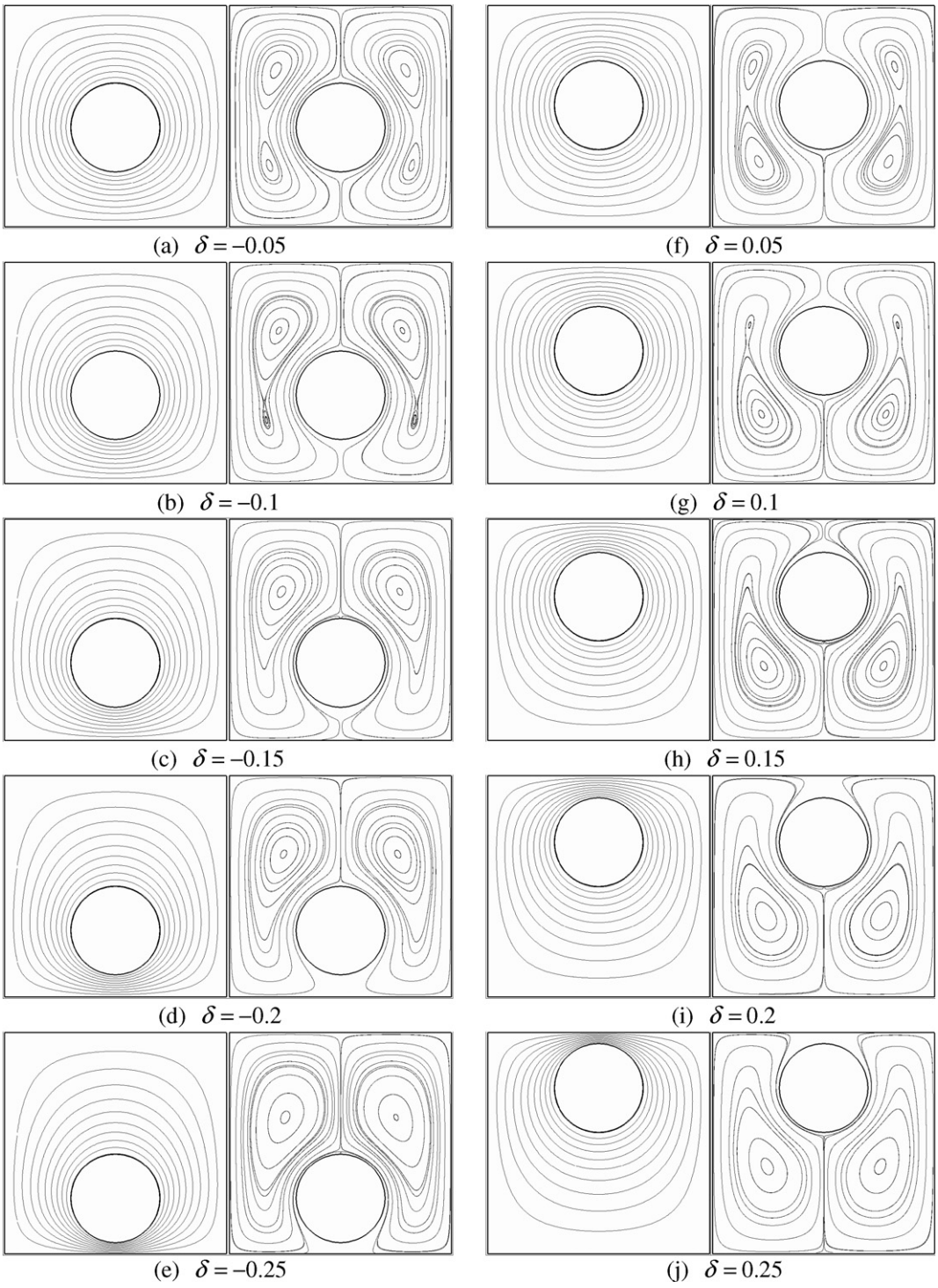

Fig. 4. Isothermals and streamlines for different δs at $Ra = 10^3$ (Contour values range from 0.1 to 1 with 10 levels).

When the cylinder moves upward, the bifurcation from the inner bi-cellular vortices to the uni-cellular vortex occurs at $\delta = 0.15$, which is later than that for the case when the cylinder moves downward. This is because a stronger convective flow exists in the region between the hot inner cylinder and top wall of the enclosure. When we increase δ further, the eyes of the two vortices move closer to the center of the enclosure and the two vortices formed in the enclosure are much more obligated than the case when the inner cylinder moves downward, which is clearly illustrated by comparing the streamlines at $\delta = -0.25$ and $\delta = 0.25$ as shown in Fig. 5e and j, respectively. Since the stronger convective flow is confined in the upper half of the enclosure, the stagnation region with

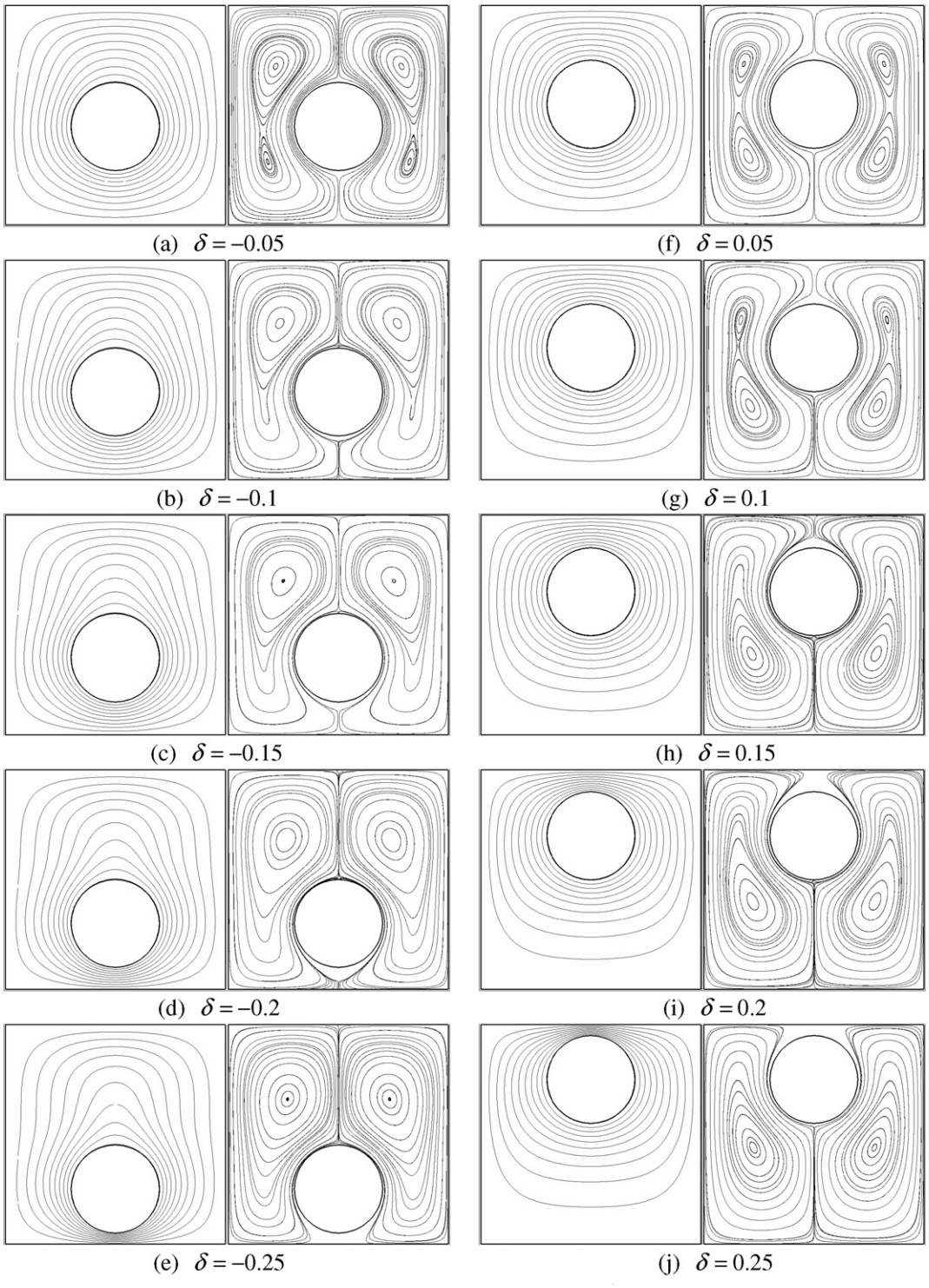

Fig. 5. Isothermals and streamlines for different δs at $Ra = 10^4$ (Contour values range from 0.1 to 1 with 10 levels).

the cold heavy fluid is formed at the bottom half, resulting in the poorer heat transfer, when the inner cylinder moves upward.

3.2.3. $Ra = 10^5$

Fig. 6 shows the distribution of isotherms and streamlines for different δs when $Ra = 10^5$. When the inner cylinder is placed at the center ($\delta = 0$) as shown in Fig. 3, the flow changes its pattern from bi-cellular vortices at $Ra = 10^3$ and 10^4 to an uni-cellular vortex at $Ra = 10^5$. When the inner cylinder moves vertically at $Ra = 10^5$, the pattern of major vortices formed in the enclosure is also uni-celluar as shown in Fig. 6, similar to the case of $\delta = 0$. The distribution of the isotherms in the enclosure

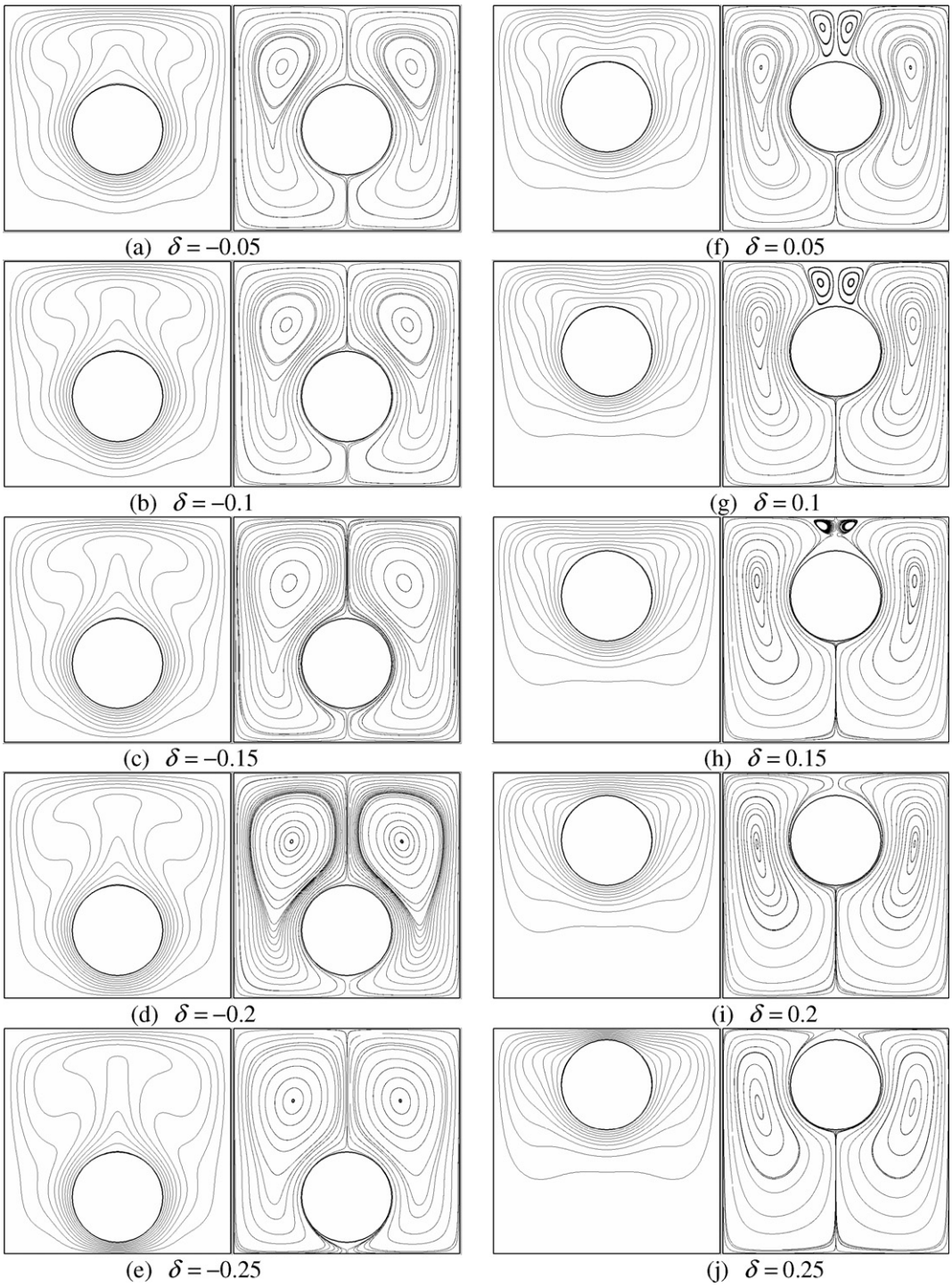

Fig. 6. Isothermals and streamlines for different δs at $Ra = 10^5$ (Contour values range from 0.1 to 1 with 10 levels).

at $Ra = 10^5$ is significantly different from that at the lower Rayleigh numbers because the buoyancy induced convection becomes more predominant than conduction.

When the inner cylinder moves downward from the center of the enclosure corresponding to the cases of Fig. 6a–e, more spaces between the hot inner cylinder and the top cold wall of the enclosure are secured, enhancing the buoyancy induced convection. Thus isotherms move upward and larger plumes exist on the top of the inner cylinder, which gives rise to the stronger thermal gradient on the top of the enclosure. The dominant flow is formed at the upper half of the enclosure, locating the core of the recirculating eddies in the upper half. The stagnant region under the inner cylinder decreases as δ becomes more negative, except for the two bottom corners of the enclosure.

When the inner cylinder moves upward, the pattern of isotherms and streamlines is much different from that when the inner cylinder moves downward. After the cylinder

moves upward from $\delta = 0.05$ where the inner cylinder is located slightly above the center of the enclosure, isotherms at the upper half of the enclosure are slightly squeezed and the temperature value at the vertical center line is lower than that at the same elevation close to the vertical centerline. Thus when $\delta = 0.05$, a plume shown in Fig. 3c at $\delta = 0.0$ is divided into three plumes as shown in Fig. 6f. Two upwelling plumes appear on the top of the inner circular cylinder at about $\pm 25°$ from the vertical centerline. A third plume appears above the top of the inner circular cylinder with reverse direction owing to the two secondary vortices newly generated over the upper part of the inner circular cylinder. As δ increases further, the reduced space above the top of the inner cylinder confines the vertical motion of flow and consequently the heat conduction is predominant over the convective heat transfer locally in this space. Thus, the secondary two vortices over the top of the inner cylinder decreases in size and finally disappears at $\delta = 0.2$, and accordingly no third plume is found at this δ. The primary symmetric eddies are squeezed and elongated vertically as the inner cylinder moves upward, which can be compared with the cases of the cylinder moving downward.

3.2.4. $Ra = 10^6$

Fig. 7 shows the distribution of isotherms and streamlines for different δs when $Ra = 10^6$. When the Rayleigh number increases to 10^6, the magnitude of the velocity circulating in the enclosure increases and the isotherms are distorted more due to the stronger convection effects, leading to the stable stratification of the isotherms. As a result the thickness of the thermal boundary formed on the surfaces of the inner cylinder and the enclosure becomes thinner and the thermal gradients on the walls become larger when $Ra = 10^6$, compared to those when $Ra = 10^5$.

When the center of the inner cylinder is placed below the center of the enclosure, $\delta < 0$, the distribution of the isotherms and streamlines for different δs shows a similar pattern with the large upwelling plumes on the top of the inner cylinder and the two main rotating symmetric eddies whose core is located at the upper half of the enclosure. When $\delta < 0$, this feature at $Ra = 10^6$ is very similar to that at $Ra = 10^5$, except that the temperature gradients formed on the surfaces of the cylinder and enclosure when $Ra = 10^6$ are sharper than those when $Ra = 10^5$. When $\delta < 0$, the vortices, which exist around the center of the bottom wall when $\delta \geqslant 0$, disappear as the space decreases between the inner cylinder and the bottom wall.

When the inner cylinder moves upward at $Ra = 10^6$, secondary vortices are formed on the top surface of the inner cylinder in addition to the main vortices, similar to the case of $Ra = 10^5$. The size of the secondary vortices at $Ra = 10^6$ is larger than that at $Ra = 10^5$ because of the stronger convection effects of the increased Rayleigh number.

When $\delta = 0.05$, we can observe the descending plume on the top surface of the inner cylinder and two ascending plumes on the upper part of the inner cylinder at the position around 30° from the vertical centerline, corresponding to the secondary vortices formed on the upper surface of the inner cylinder. When $\delta = 0.05$, the size of the secondary vortices and the distance from the vertical centerline to the ascending plume at $Ra = 10^6$ become larger, compared to those at $Ra = 10^5$, due to the increasing convection effects with the increasing Rayleigh number. When $\delta = 0.05$ at $Ra = 10^6$, we can also observe the formation of additional vortices on the bottom wall of the enclosure, which is not present when $\delta < 0$ at the same Rayleigh number. The size of the vortices formed on the bottom wall and the distance from the center to the separation point at $\delta = 0.05$ becomes larger, compared to those at $\delta = 0$.

When δ increases further to 0.1 and 0.15, the isotherms are a little squeezed as the space decreases between the inner cylinder and the top wall of the enclosure, but the shapes of the isotherms and streamlines are generally similar to those at $\delta = 0.05$. The size of the secondary vortices formed on the upper surface of the inner cylinder at $\delta = 0.1$ and 0.15 is smaller than that at $\delta = 0.05$, whereas the size of the additional vortices formed on the bottom wall becomes larger, compared to those at $\delta = 0.05$.

At $\delta = 0.2$, at $Ra = 10^5$, the secondary vortices on the upper surface of the inner cylinder disappear as shown in Fig. 6i. However, as the Rayleigh number increases to 10^6 at $\delta = 0.2$, the tertiary vortices are formed on the top surface of the inner cylinder in addition to the secondary vortices with the presence of three upwelling and two downwelling plumes on the upper surface of inner cylinder, even though the space between the inner cylinder and the top wall of the enclosure becomes smaller, as shown in Fig. 7i. The additional vortices which are present on the bottom wall at $0 \leqslant \delta \leqslant 0.15$ disappear at $\delta = 0.2$, because the convective flow is not strong enough to penetrate the increased space below the bottom of the inner cylinder and as a result the separation of the boundary layer on the bottom wall doesn't occur.

When $\delta = 0.25$, the space between the inner cylinder and the top wall of the enclosure is very small. As a result the two pairs of the vortices formed on the upper surface of the inner cylinder at $\delta = 0.2$ merge into a pair of secondary vortices. Thus there are a single downwelling and two upwelling plumes on the upper surface of the inner cylinder. The shape of the main vortices at $\delta = 0.25$ is generally similar to that at $\delta = 0.2$.

3.3. Trajectory of the center of the rotating eddies as a function of δ

Fig. 8 shows the trajectory of the center of the main rotating vortices in the $x - y$ plane for different δs at four different Rayleigh numbers. Since the flow and thermal fields are symmetric about the vertical center line at $x = 0$, the trajectories of the center of the vortices in the right half of the enclosure are depicted in Fig. 8. As mentioned above, the bifurcation from the bi-cellular vortices to the uni-cellular vortex occur at the low Rayleigh numbers of 10^3 and 10^4.

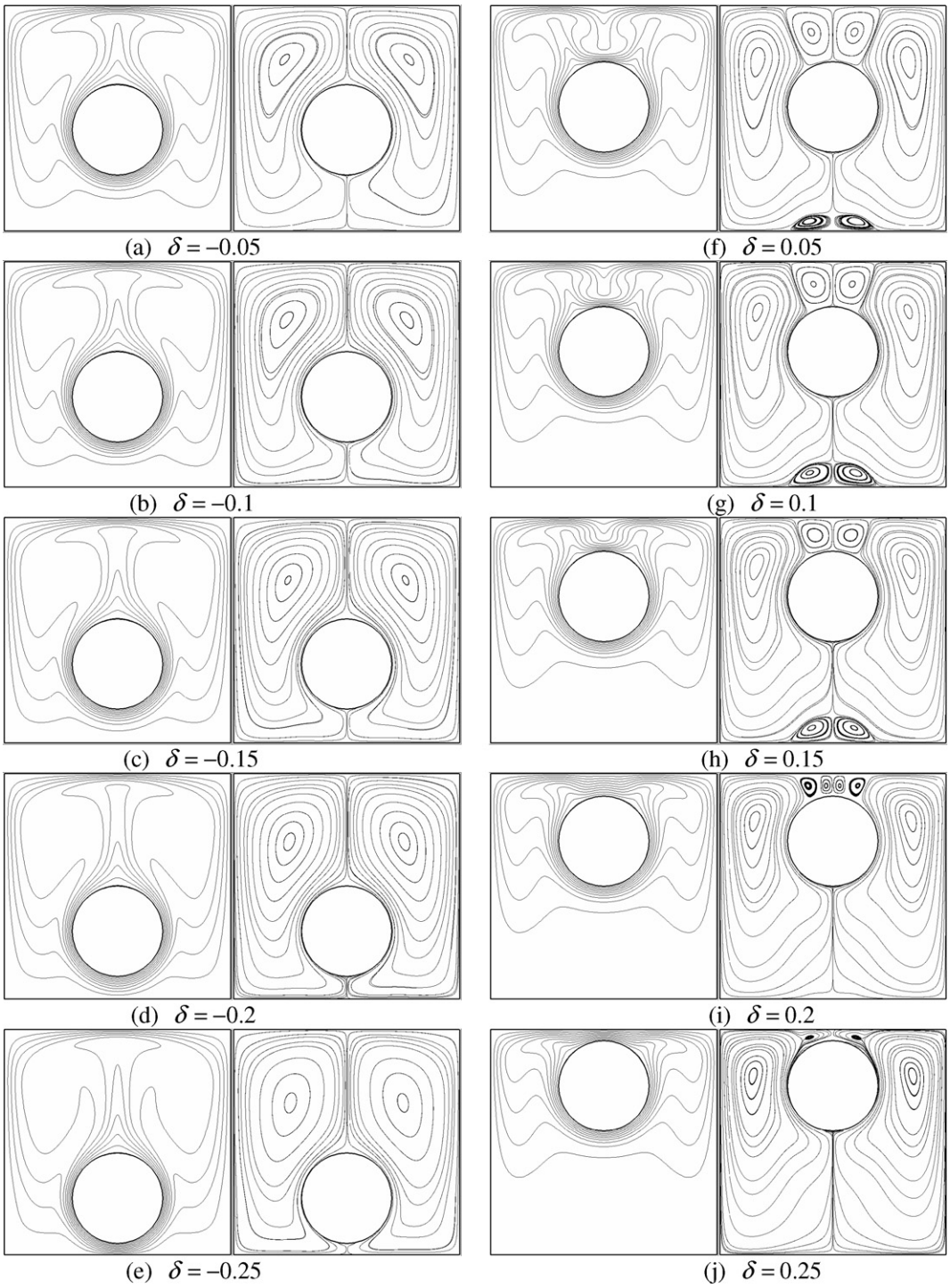

Fig. 7. Isothermals and streamlines for different δs at $Ra = 10^6$ (Contour values range from 0.1 to 1 with 10 levels).

The bi-cellular vortices with two inner vortices in the upper and lower half regions appear in the range of $-0.1 \leqslant \delta \leqslant 0.1$ when $Ra = 10^3$ and $-0.05 \leqslant \delta \leqslant 0.1$ when 10^4, respectively. At these low Rayleigh numbers, flow is strongly confined by the size of the space depending on the location of the inner cylinder because of weak convection. As a result, when the inner cylinder is close to the bottom wall, the increased space over the top of the inner cylinder leads to form the flow in the upper half. The opposite is also true as shown in Figs. 4 and 5 at $Ra = 10^3$ and 10^4, respectively. Thus, at theses lower Rayleigh numbers, the two trajectories are plotted in the upper half and lower half, respectively, as show in Fig. 8a and b.

When $Ra = 10^3$, the trajectory of vortex center at the upper half region is almost symmetric to that at the lower half region with respect to the horizontal center line at

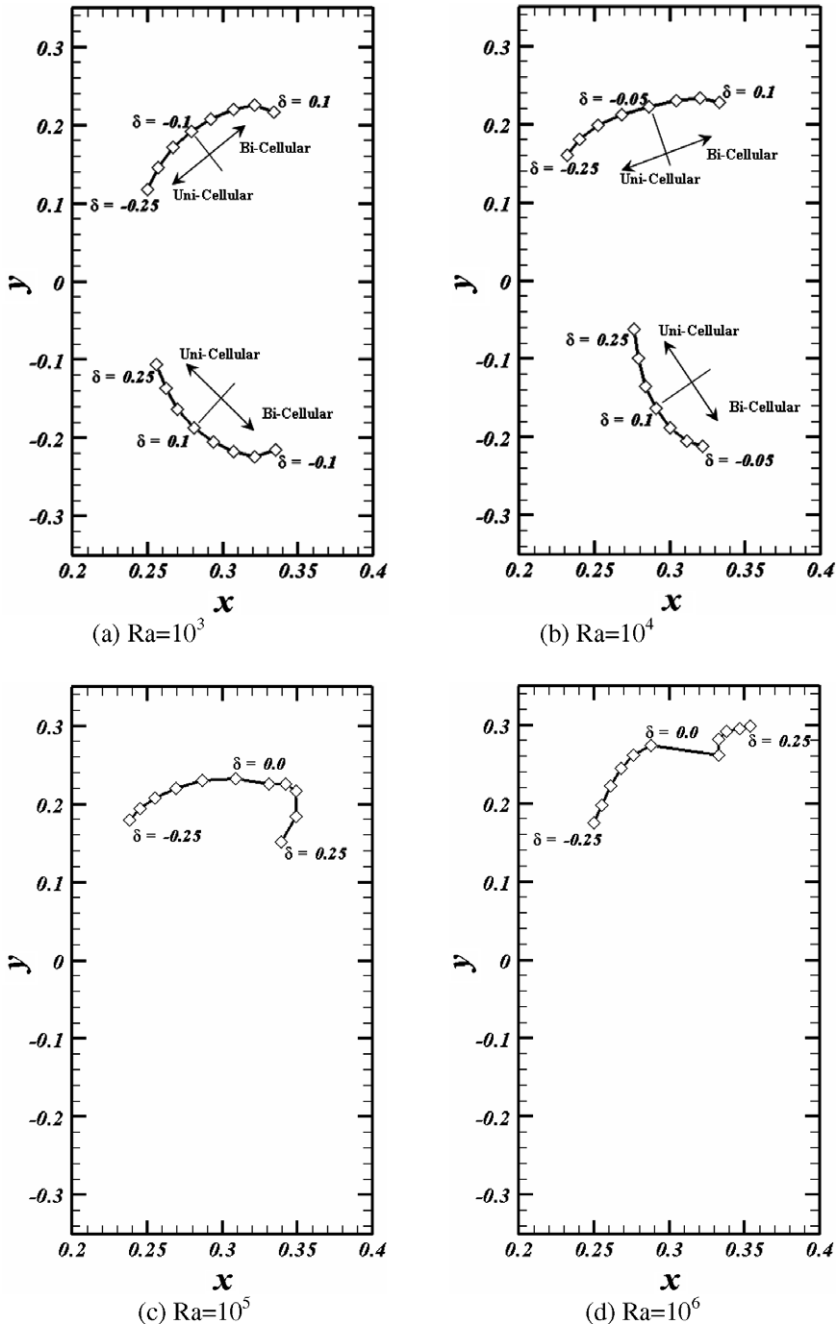

Fig. 8. Trajectories of the center of overall rotating eddy in the $x - y$ plane at the different positions of the inner cylinder at four different Rayleigh numbers.

$y = 0$. The trajectory of the upper vortex center shown at the upper part of Fig. 8a corresponds to the location of upper inner vortex center of the bi-cellular vortices when $-0.1 \leqslant \delta \leqslant 0.1$ and that of the uni-cellular vortex when $-0.25 \leqslant \delta \leqslant -0.15$. When we increase δ from -0.25 to 0.1, meaning that the distance between the inner cylinder and the bottom wall becomes larger, the center of the upper inner vortices moves upward and outward, and becomes more distant from the origin of the enclosure. Similarly, the trajectory of lower vortex center shown at the lower part of Fig. 8 corresponds to the location of the lower inner vortex center of the bi-cellular vortices when $-0.1 \leqslant \delta \leqslant 0.1$ and that of the uni-cellular vortex when $0.15 \leqslant \delta \leqslant 0.25$. When we increase δ from -0.1 to 0.25, the center of the lower inner vortices moves upward and inward, and becomes closer to the origin of the enclosure.

When $Ra = 10^4$, the trajectory of vortex center at the upper half of the region is not symmetric to that at the lower half of the region with respect to the horizontal center line at $y = 0$ unlike the case with $Ra = 10^3$, due to the increasing effect of convection with the increasing Rayleigh number. The trajectory of the upper vortex center shown at

the upper part of Fig. 8b corresponds to the location of the upper inner vortex center of the bi-cellular vortices when $-0.05 \leqslant \delta \leqslant 0.1$ and that of the uni-cellular vortex when $-0.25 \leqslant \delta \leqslant -0.1$. When we increase δ from -0.25 to 0.1 at $Ra = 10^4$, the center of the upper inner cylinder moves less upward with a smaller variation in the vertical direction and moves more outward with a larger variation in the horizontal direction, compared to the movement at $Ra = 10^3$. The trajectory of the lower vortex center shown at the lower part of Fig. 8b corresponds to the location of the lower inner vortex center of the bi-cellular vortices when $-0.05 \leqslant \delta \leqslant 0.1$ and that of the uni-cellular vortex when $0.15 \leqslant \delta \leqslant 0.25$. When we increase δ from -0.05 to 0.25 at $Ra = 10^4$, the center of the lower inner vortices moves more upward with a larger variation in the vertical direction and less inward with a smaller variation in the horizontal direction, compared to the movement at $Ra = 10^3$, showing clearly the increasing convection effect with increasing Rayleigh number.

Unlike the cases of lower Rayleigh numbers of 10^3 and 10^4, the main vortices formed in the enclosure when $Ra = 10^5$ and 10^6 have only the uni-cellular form due to the stronger convection effect and the centers of the inner vortices are located at the upper half of the region of the enclosure for all δs.

When we increase δ from -0.25 to 0 at $Ra = 10^5$, meaning that the distance between the inner cylinder and the bottom wall becomes larger, the center of the inner vortices moves upward and outward, and becomes more distant from the origin of the enclosure, as shown in Fig. 8c. When we increase δ further from 0 to 0.15, the center of the inner vortices keeps moving outward without any significant variations in the vertical direction due to the presence of the secondary vortices on the upper surface of the inner cylinder as shown in Fig. 6. If we increase δ to 0.2 and 0.25, the secondary eddies on the upper surface disappear and the center of the inner vortices moves downward and inward with a relatively large variation in both the vertical and horizontal directions.

When we increase δ from -0.25 to 0 at $Ra = 10^6$, the center of the inner vortices moves upward with larger variation in the vertical direction and outward with smaller variation in the horizontal direction than the variation at $Ra = 10^5$, as shown in Fig. 8d. When we increase δ from 0 to 0.05, the center of the inner vortices moves outward with a large variation in the horizontal direction and downward with a small variation in the vertical direction, due to the presence of secondary vortices on the upper surface of the inner cylinder and additional vortices on the bottom wall as shown in Fig. 7. When we increase δ further from 0.05 to 0.25, the center of the inner vortices keeps moving upward and outward.

3.4. Local Nusselt number

3.4.1. $Ra = 10^3$

Fig. 9 shows the distribution of local Nusselt numbers along the hot surface of the inner cylinder and the cold surfaces of the enclosure for different δs at $Ra = 10^3$. The distribution of the local Nusselt numbers only in the right half of the enclosure and inner cylinder is shown in Fig. 9 because of a two-fold symmetry about the vertical center line at $x = 0$.

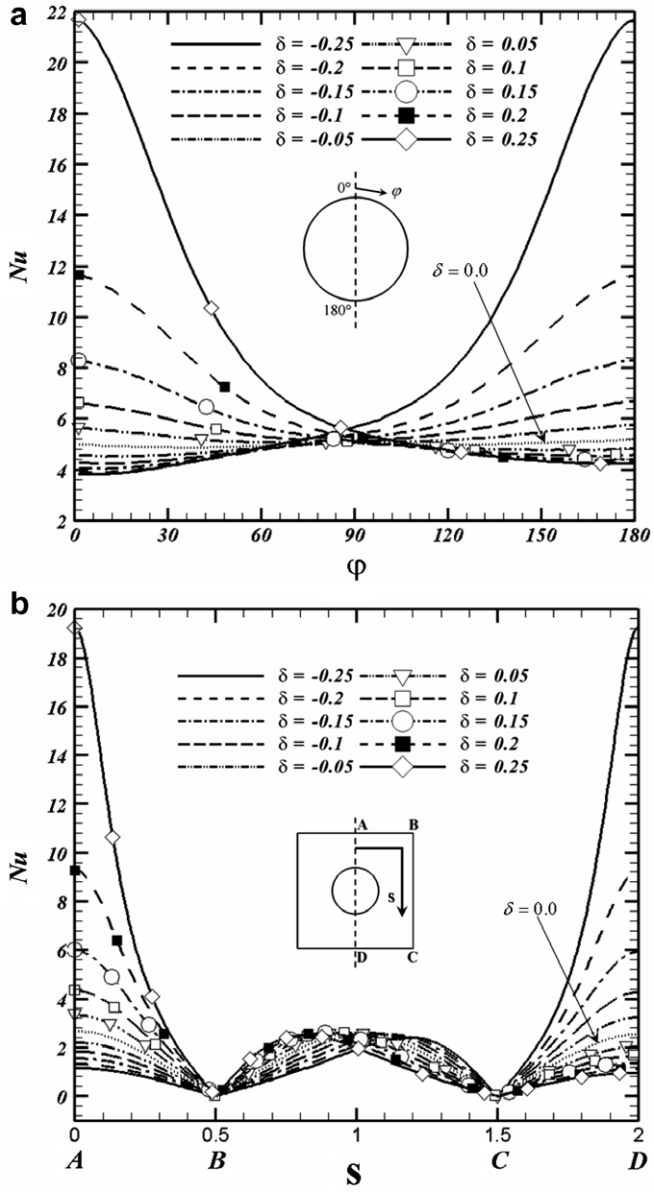

Fig. 9. Local Nusselt number distribution along (a) the surface of the inner cylinder and (b) the surfaces of the enclosure at different positions of the inner cylinder for $Ra = 10^3$.

When $\delta = 0$ where the inner cylinder is located at the center of the enclosure at $Ra = 10^3$, the isotherms show almost a symmetric shape with respect to the horizontal centerline at $y = 0$ because the dominant effect is conduction as shown in Fig. 3a, and as a result the distribution of the local Nusselt numbers along the surface of the inner cylinder and cold surface of the enclosure shows the symmetric shape with respect to $\varphi = 90°$ and $y = 0$. When $\delta = 0$, the variation of the local Nusselt numbers along

the hot surface of the inner cylinder is very small. However, the distribution of the local Nusselt numbers has a relatively large variation along the cold surface of the enclosure, compared to that along the hot surface of the inner cylinder. The local Nusselt number has a maximum value at point A which is the stagnation point on the top wall of the enclosure. When we move from point A to B along the top wall of the enclosure, the local Nusselt number decreases and reaches a local minimum value close to zero at point B. When we move from point B to C along the right wall of the enclosure, the local Nusselt number increases, reaches a local maximum value at $s = 1$ where s is the distance from point A along the surfaces of the enclosure, and decreases again until it has a local minimum value at point C. When we move further from point C to D, the local Nusselt number increases slightly again.

When the inner cylinder moves upward or downward at $Ra = 10^3$, the symmetry of isotherms with respect to $\varphi = 90°$ and $y = 0$ is broken as shown in Fig. 4 and as a result the symmetry of the local Nusselt numbers is also broken. As the inner cylinder moves upward with increasing the value of δ, the space between the inner cylinder and the top wall decreases whereas the space between the inner cylinder and the bottom wall increases. As a result, with increasing value of δ, the gradient of isotherms and their corresponding distribution of local Nusselt numbers at $0° \leqslant \varphi \leqslant 90°$ increase whereas those at $90° \leqslant \varphi \leqslant 180°$ decrease, compared to those when $\delta = 0$. The local Nusslet number along the cold surfaces of the enclosure shows a similar pattern with increasing δ. As δ increases, the local Nusselt numbers along the cold surface at the upper half of the enclosure of $0 \leqslant s \leqslant 1$ increases whereas that at the lower half of the enclosure of $1 \leqslant s \leqslant 2$ decrease, compared to those when $\delta = 0$. The variation of the local Nusselt number values along the top surface of the enclosure (region A–B) according to the variation of δ is very large whereas that along the left surface (region B–C) and the bottom surface (region C–D) is relatively small, due to the distribution of isotherms shown in Fig. 4.

When the inner cylinder moves downward at $Ra = 10^3$ with an increasing absolute value of δ, the distribution of the local Nusselt numbers along the hot surface of the inner cylinder and cold surface of the enclosure shows almost symmetric shapes with respect to $\varphi = 0°$ and $s = 1$ because the distribution of isotherms when $\delta < 0$ is almost symmetric to that when $\delta > 0$ with respect to $y = 0$.

3.4.2. $Ra = 10^4$

Fig. 10 shows the distribution of local Nusselt numbers along the hot surface of the inner cylinder and the cold surfaces of the enclosure for different δs at $Ra = 10^4$. The values of the local Nusselt numbers at $Ra = 10^4$ are larger than those at $Ra = 10^3$, due to increasing effect with increasing Rayleigh number.

The distribution of the local Nusselt numbers along the hot surface of the inner cylinder and cold surface of the enclosure when $\delta = 0$ at $Ra = 10^4$ is not symmetric any more with respect to $\varphi = 90°$ and $y = 0$ due to the effect of convection, unlike the case when $\delta = 0$ at $Ra = 10^3$. The local Nusselt number at $\delta = 0$ increases with increasing φ because the isotherms move upward slightly in the presence of convection, meaning that the local Nusselt number at the lower surface of the inner cylinder is larger than that at the upper surface of the inner cylinder. The variation of the local Nusslet number along the surface of the enclosure at $\delta = 0$ for $Ra = 10^4$ is similar to that for $Ra = 10^3$, even though the symmetry about $s = 1$ is slightly broken.

In the region where the local Nusselt number at $\delta > 0$ is larger than that at $\delta = 0$ at $Ra = 10^4$, the variation of the local Nusselt numbers according to the variation of δ has a similar pattern to that at $Ra = 10^3$ and their values

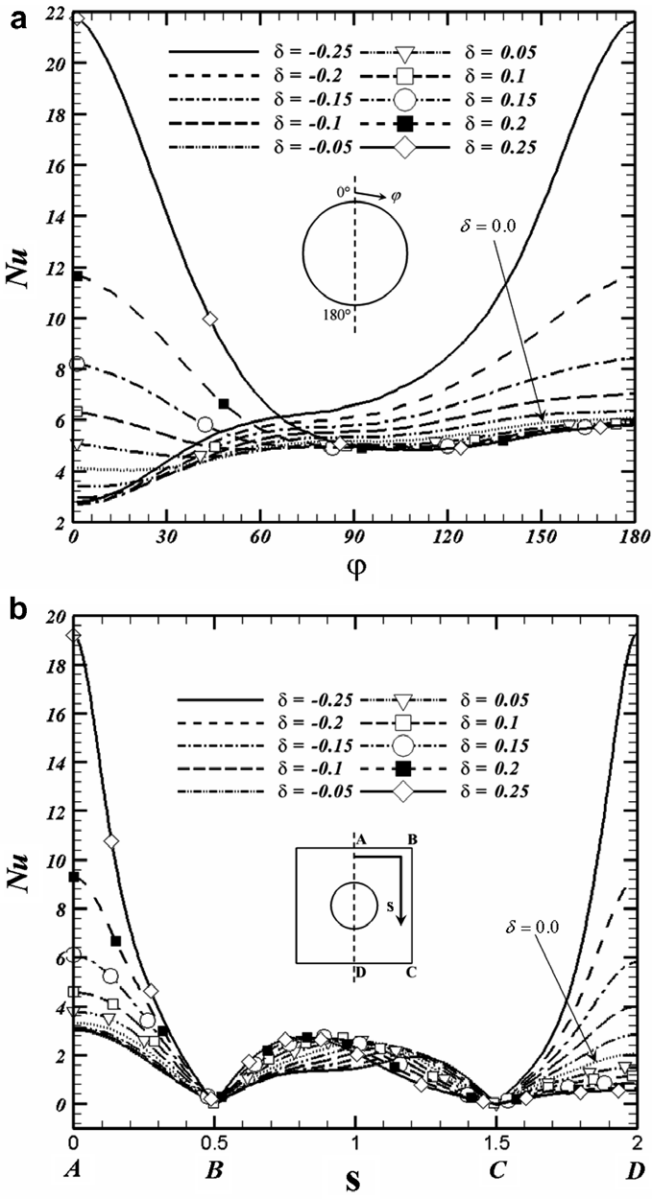

Fig. 10. Local Nusselt number distribution along (a) the surface of the inner cylinder and (b) the surfaces of the enclosure at different positions of the inner cylinder for $Ra = 10^4$.

increase with increasing δ. The position where the local Nusselt number at $\delta > 0$ is equal to that at $\delta = 0$ when $Ra = 10^4$ is different from that when $Ra = 10^3$ and moves to the upper position of the inner cylinder. In the region where the local Nusselt number at $\delta > 0$ is smaller than that at $\delta = 0$ at $Ra = 10^4$, the variation of the local Nusselt number according to the variation of δ is very small.

When the cylinder moves downward at $Ra = 10^4$, the local Nusselt number at $\delta < 0$ is larger than that $\delta = 0$ in most regions along the surface of the inner cylinder except in the region close to the top surface of the inner cylinder due to the presence of rising plume in this region. In the region where the local Nusselt number at $\delta < 0$ is larger than that at $\delta = 0$ at $Ra = 10^4$, the variation of the local Nusselt numbers according to the variation of δ has a similar pattern to that at $Ra = 10^3$ and their values increase with an increasing absolute value of δ. The position where the local Nusselt number at $\delta < 0$ is equal to that at $\delta = 0$ when $Ra = 10^4$ moves to the upper position of the inner cylinder close to $\varphi = 0°$. The shape of the local Nusselt number distribution along the cold surface of the enclosure for $\delta \leqslant 0$ at $Ra = 10^4$ is generally similar to that at $Ra = 10^3$. Some differences are shown in the right wall of the enclosure of $0.5 \leqslant s \leqslant 1.5$. The location of the local Nusselt number maxima is not at $s = 1$ but increases to the bottom wall direction.

3.4.3. $Ra = 10^5$

Fig. 11 shows the distribution of the local Nusselt numbers along the hot surface of the inner cylinder and the cold surfaces of the enclosure for different δs at $Ra = 10^5$. The values of the local Nusselt numbers at $Ra = 10^5$ is larger than that at $Ra = 10^3$ and 10^4, due to the increasing effect of convection with increasing Rayleigh number.

When the inner cylinder moves upward at $Ra = 10^5$, the local Nusselt number on the surface of the inner cylinder has a maximum value at the top of the inner cylinder of $\varphi = 0°$ due to the increasing thermal gradient with decreasing space between the inner cylinder and the top wall of the enclosure. As φ increases from the top of the inner cylinder, due to the presence of the rising plume on the surface of the inner cylinder, the local Nusselt number on the surface of the inner cylinder for $\delta > 0$ decreases until it has a minimum value and then increases again. The location, in which the local Nusselt number has a minimum value on the surface of the inner cylinder, becomes more distant from the top of the inner cylinder with increasing δ, because the rising thermal plume on the surface of the inner cylinder moves to the increasing φ direction. As φ increases from the position where the local Nusselt number has a minimum value, the value of the local Nusselt number at $\delta > 0$ is smaller than that at $\delta = 0$ and the difference in the local Nusselt numbers between $\delta = 0$ and $\delta > 0$ keeps decreasing as shown in Fig. 11.

When $\delta = 0.05$, 0.1 and 0.15 at $Ra = 10^5$, the secondary eddies are formed on the upper surface of the inner cylinder due to the presence of upwelling and downwelling plumes.

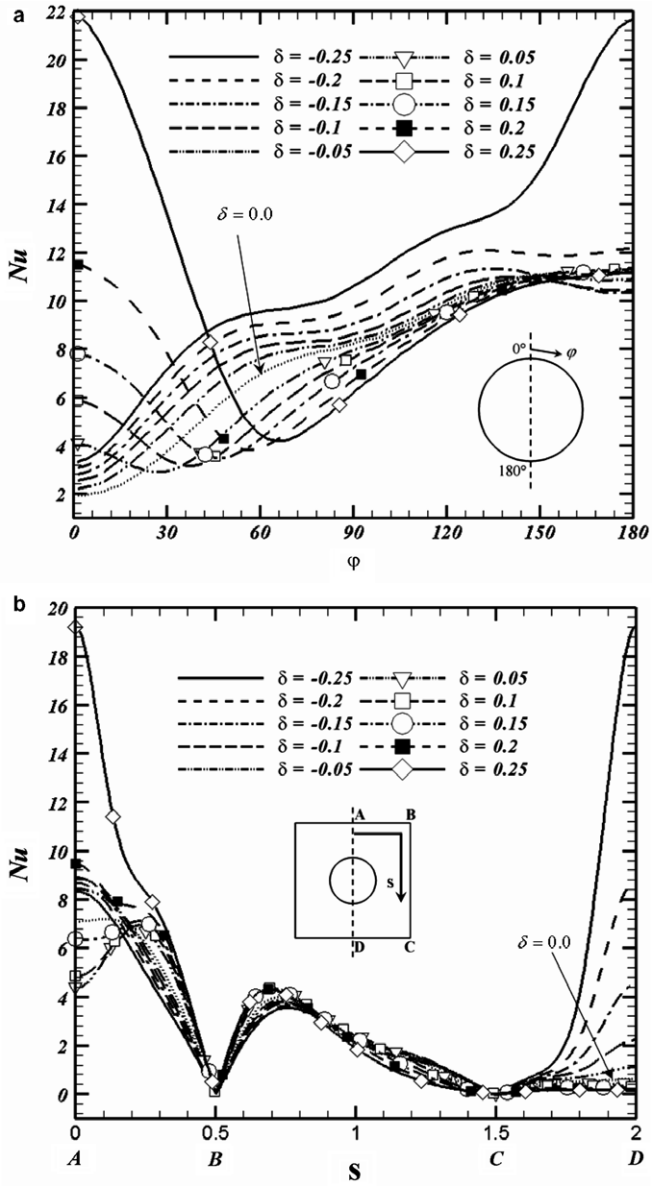

Fig. 11. Local Nusselt number distribution along (a) the surface of the inner cylinder and (b) the surfaces of the enclosure at different positions of the inner cylinder for $Ra = 10^5$.

Thus the local Nusselt number at $s = 0$ (point A) on the cold surface of the enclosure when $\delta = 0.05$, 0.1 and 0.15 is not the maximum in the presence of downwelling plume unlike to the cases of $Ra = 10^3$ and 10^4. When we move from the point A to point B along the top wall of the enclosure at $\delta = 0.05$, 0.1 and 0.15, the local Nusselt number increases until it has a maximum value at the location with the upwelling plume and then decreases until it has a minimum value at $s = 0.5$ (point B). In the region A–B along the surface of the enclosure, the value of the local Nusselt number when $\delta = 0.05$, 0.1 and 0.15 is smaller than that when $\delta = 0$. When δ increases to 0.2 and 0.25, the space between the inner cylinder and the top wall of the enclosure becomes smaller and the secondary eddies disappear. As a result, when $\delta = 0.2$ and 0.25, the local Nusselt number at

$s = 0$ has a maximum value and decreases as we move from the point A to B until it has a minimum value at $s = 0.5$. In the region A–B along the surface of the enclosure, the value of the local Nusselt number when $\delta = 0.2$ and 0.25 is larger than that when $\delta = 0$ and increases with increasing δ. When we move from point B ($s = 0.5$) to point C ($s = 1.5$) at $\delta > 0$, the local Nusselt number on the surface of the enclosure increases until it has the maxima and then keeps decreasing until it has a minimum value at $s = 1.5$. The local Nusselt number at $\delta > 0$ does not change much and has an almost constant value close to zero, because the region C–D becomes stagnant when the inner cylinder moves upward. When the inner cylinder moves upward, the variation of the local Nusselt numbers in the region of $0.5 \leqslant s \leqslant 1.5$ is very small because the distribution of isotherms is similar in this region as shown in Fig. 6.

When the inner cylinder moves downward at $Ra = 10^5$, the local Nusselt number along the surface of the inner cylinder increases generally with increasing φ and has similar patterns for different δs because the distribution of isotherms around the surface of the inner cylinder is similar as $\delta \geqslant 0$ as shown in Fig. 6a–e. Due to the presence of a rising plume on the upper surface of the inner cylinder, the local Nusselt number at $\delta \leqslant 0$ increases rapidly in the region around $0 \leqslant \varphi \leqslant 60°$ followed by a slow increase in the region around $60° \leqslant \varphi \leqslant 90°$. When we move further in the increasing φ direction for different δ values of -0.05, -0.1, -0.15 and -0.2, the local Nusselt numbers increase rapidly again around $90° \leqslant \varphi \leqslant 130°$ followed by the slow decrease in the region around $130° \leqslant \varphi \leqslant 180°$. However, when $\delta = -0.25$, the local Nusselt numbers increase very rapidly in the region around $130° \leqslant \varphi \leqslant 180°$ unlike the cases at $-0.2 \leqslant \delta \leqslant 0$ because the isotherms are squeezed due to the very small space between the inner cylinder and the bottom wall.

When the inner cylinder moves downward at $Ra = 10^5$, the local Nusselt number along the surface of the enclosure is different from that when the inner cylinder moves upward. Because the secondary vortices do not exist on the upper surface of the inner cylinder, the local Nusselt number at $\delta < 0$ has a maximum value at $s = 0$ (point A) and decreases as we move from point A to point B until it has a minimum value at $s = 0.5$ (point B). As the inner cylinder moves downward, the local Nusselt number in the region of $0 \leqslant s \leqslant 0.5$ decreases with an increasing absolute value of δ because the gradient of the isotherms on the top wall becomes smaller with increasing gap between the inner cylinder and the top wall of the enclosure. However the variation of the local Nusselt numbers along the top wall of the enclosure for different δs is not large when $\delta < 0$. 'The local Nusselt number in the region of $0.5 \leqslant s \leqslant 1.5$ at $\delta < 0$ has a similar distribution to that at $\delta > 0$. The difference in the value of the local Nusselt numbers in the region of $0.5 \leqslant s \leqslant 1.5$ is not large for all the different values of δ. When we move from point C to point D along the bottom wall, the local Nusselt numbers at $\delta < 0$ increases with increasing s. The local Nusselt number on the bottom wall also increases very rapidly with increasing absolute value of δ at $\delta < 0$ because the gap between the inner cylinder and the bottom wall keeps decreasing and the gradient of isotherms on the bottom wall increases very rapidly when the inner cylinder keeps moving downward.

3.4.4. $Ra = 10^6$

Fig. 12 shows the distribution of local Nusselt numbers along the hot surface of the inner cylinder and the cold surfaces of the enclosure for different δs at $Ra = 10^6$. The values of the local Nusselt number at $Ra = 10^6$ are larger than those at $Ra = 10^3$, 10^4 and 10^5, due to the strong effect of convection with increasing Rayleigh number.

When the inner cylinder moves downward at $Ra = 10^6$, the pattern of the local Nusselt number variation along the

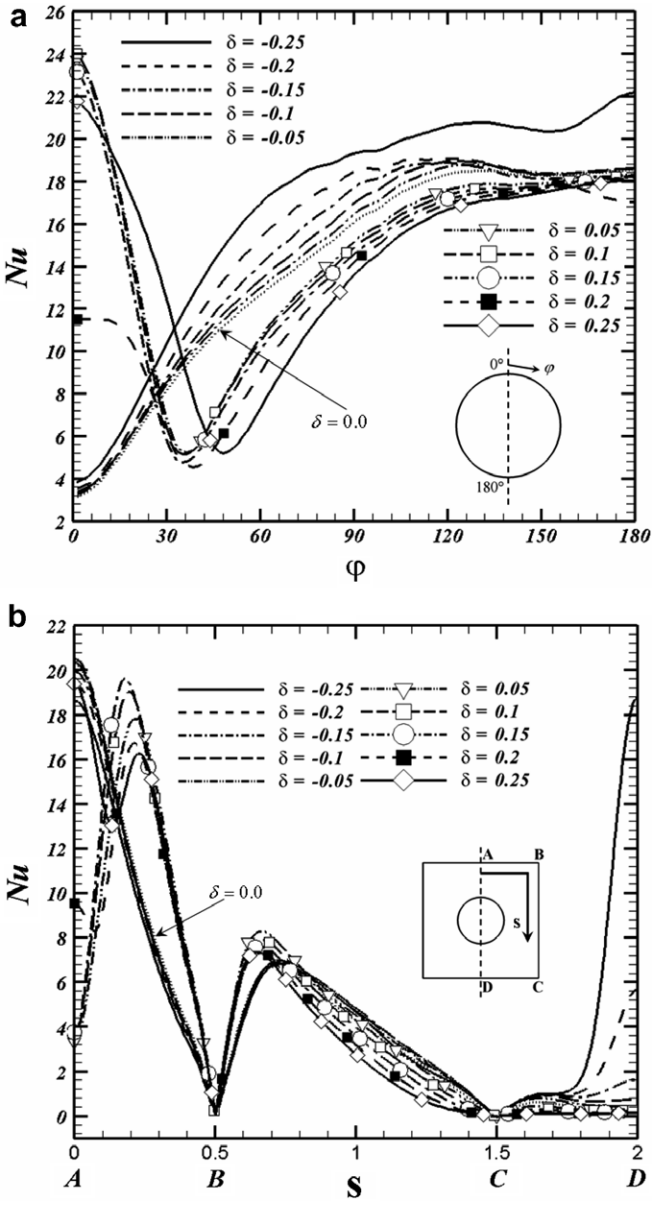

Fig. 12. Local Nusselt number distribution along (a) the surface of the inner cylinder and (b) the surfaces of the enclosure at different positions of the inner cylinder for $Ra = 10^6$.

surface of the inner cylinder is similar to the case of $Ra = 10^5$. As we move along the surface of the inner cylinder to the increasing φ direction when $\delta > 0$, the local Nusselt number decreases from the maxima at $\varphi = 0$ until it has a minimum value around the location of the rising plume, followed by the increase of its value, due to the presence of secondary and tertiary vortices on the upper surface of the inner cylinder. The local Nusselt number at $\varphi = 0$ has the largest value at $\delta = 0.05$ and decreases with increasing δ because the size of the secondary vortices formed on the upper surface of the inner cylinder at $\delta = 0.05$ is larger than that at $\delta \geqslant 0.1$. Even though the secondary vortices almost disappear on the upper surface of the inner cylinder when $\delta = 0.25$, the value of the local Nusselt number at $\varphi = 0$ for $\delta = 0.25$ is larger than that for $\delta = 0.2$ because the space between the inner cylinder and the top wall is small and the isotherms are squeezed, resulting in a very dense thermal gradient at $\varphi = 0$. In the region where the local Nusselt number increases with increasing φ, the local Nusselt number on the surface of the inner cylinder at $\delta > 0$ is smaller than that at $\delta = 0$ and decreases with increasing δ.

When the inner cylinder moves downward at $Ra = 10^6$, due to the presence of the secondary and tertiary vortices on the upper surface of the inner cylinder, the local Nusselt number in the region of $0 \leqslant s \leqslant 0.5$ increases until it has a maximum value around the location where the upwelling plume impinges on the top wall of the enclosure and decreases until it reaches the minimum value at $s = 0.5$. The maximum value of the local Nusselt number in the region of $0 \leqslant s \leqslant 0.5$ increases with increasing δ from 0.05 to 0.15, has the largest value at $\delta = 0.15$ and decreases with increasing δ from 0.15 to 0.25, due to the interaction between the rising plume from the upper surface of the inner cylinder and the top wall. The general shape of the variation of the local Nusselt number according to the variation of s in the region of $0.5 \leqslant s \leqslant 1.5$ when $Ra = 10^6$ is similar to that when $Ra = 10^5$. However, the value of the maxima in the region of $0.5 \leqslant s \leqslant 1.5$ when $Ra = 10^6$ is much larger than that when $Ra = 10^5$ due to the stronger convection effects with increasing Rayleigh number.

When the inner cylinder moves downward at $Ra = 10^6$, the general trend of the local Nusselt number variation along the surfaces of both the inner cylinder and the enclosure is similar to that when $Ra = 10^5$. Compared to the distribution of the local Nusselt number along the surface of the inner cylinder when $\delta < 0$ at $Ra = 10^5$, some minor differences are observed when $\delta = -0.25$ at $Ra = 10^6$. When $\delta = -0.25$ at $Ra = 10^5$, the local Nusselt number around the bottom surface of the inner cylinder increases very rapidly as shown in Fig. 11. However, when $\delta = -0.25$ at $Ra = 10^6$, we can observe a very small variation of the local Nusselt number in this region unlike the case at $Ra = 10^5$, because the strong convection at $Ra = 10^6$ forces the isotherms around the bottom surface of the inner cylinder to maintain a similar pattern to that at $-0.2 \leqslant \delta \leqslant -0.05$, even though the gap between the inner cylinder and the bottom wall is very small at $\delta = -0.25$. We can also observe some differences on the surface of the enclosure. Because the effect of convection is very strong at $Ra = 10^6$, the local Nusslet number in the region of $0 \leqslant s \leqslant 0.5$ at $Ra = 10^6$ is much bigger than that at $Ra = 10^5$. The location for the maxima of the local Nusselt number in the region of $0.5 \leqslant s \leqslant 1.5$ at $Ra = 10^6$ moves slightly upward, compared to that at $Ra = 10^5$.

3.5. Surface-averaged Nusselt number

Fig. 13a shows the surface-averaged Nusselt number at the top wall of the enclosure, $\overline{Nu}_T$, as a function of δ for different Rayleigh numbers. $\overline{Nu}_T$ increases generally with increasing Rayleigh number due to the increasing effect of convection.

When $Ra = 10^3$, the surface-averaged Nusslet number at the top wall depends on the variation of δ very much and increases very rapidly with increasing δ. When the inner cylinder is placed at the lower half of the enclosure with a negative value of δ at $Ra = 10^4$, $\overline{Nu}_T$ increases very slowly with increasing δ, meaning that $\overline{Nu}_T$ does not depend much on the variation of δ at $\delta < 0$ due to increasing effect of convection with increasing Rayleigh number. However, when $\delta > 0$ at $Ra = 10^4$, $\overline{Nu}_T$ increases very rapidly due to the increasing effect of δ. Thus, if the distance from the inner cylinder to the top wall decreases with increasing δ, the difference in the value of $\overline{Nu}_T$ between $Ra = 10^3$ and 10^4 decreases and $\overline{Nu}_T$ at $Ra = 10^4$ is almost the same as that at $Ra = 10^3$ when $\delta = 0.2$ and 0.25.

When δ increases from -0.25 to -0.05 at $Ra = 10^5$, $\overline{Nu}_T$ increases slowly due to the slight increase in thermal gradient on the top wall of the enclosure with decreasing distance between the inner cylinder and the top wall with increasing δ and the dependence of $\overline{Nu}_T$ on δ is very low in this region. However, when δ increases to 0 and 0.05 at $Ra = 10^5$, the strength of the rising thermal plume formed around the top surface of the inner cylinder decreases and the secondary vortices are formed on the top surface of the inner cylinder. As a result $\overline{Nu}_T$ decreases slightly when $\delta = 0$ and 0.05 at $Ra = 10^5$. If δ increases further to values larger than 0.1, the effect of δ becomes more dominant even though secondary vortices exist on the upper surface of the inner cylinder and as a result $\overline{Nu}_T$ increases again rapidly with increasing δ.

The variation of $\overline{Nu}_T$ at $Ra = 10^6$ is generally similar to that at $Ra = 10^5$. When δ increases at $Ra = 10^6$, $\overline{Nu}_T$ increases slowly at $-0.25 \leqslant \delta \leqslant 0$, decreases at $\delta = 0.05$ due to the presence of the strong secondary vortices on the upper surface of the inner cylinder, and increases again at $0.05 \leqslant \delta \leqslant 0.15$ due to the increasing effect of the distance between the inner cylinder and the top wall of the enclosure in the presence of the secondary vortices. When $\delta = 0.2$ at $Ra = 10^6$, $\overline{Nu}_T$ decreases again because the presence of the secondary and tertiary vortices on the upper surface of the inner cylinder gives more dominant effect on $\overline{Nu}_T$ than δ. When $\delta = 0.25$ at $Ra = 10^6$, $\overline{Nu}_T$ increases to the maximum value because the distance between the

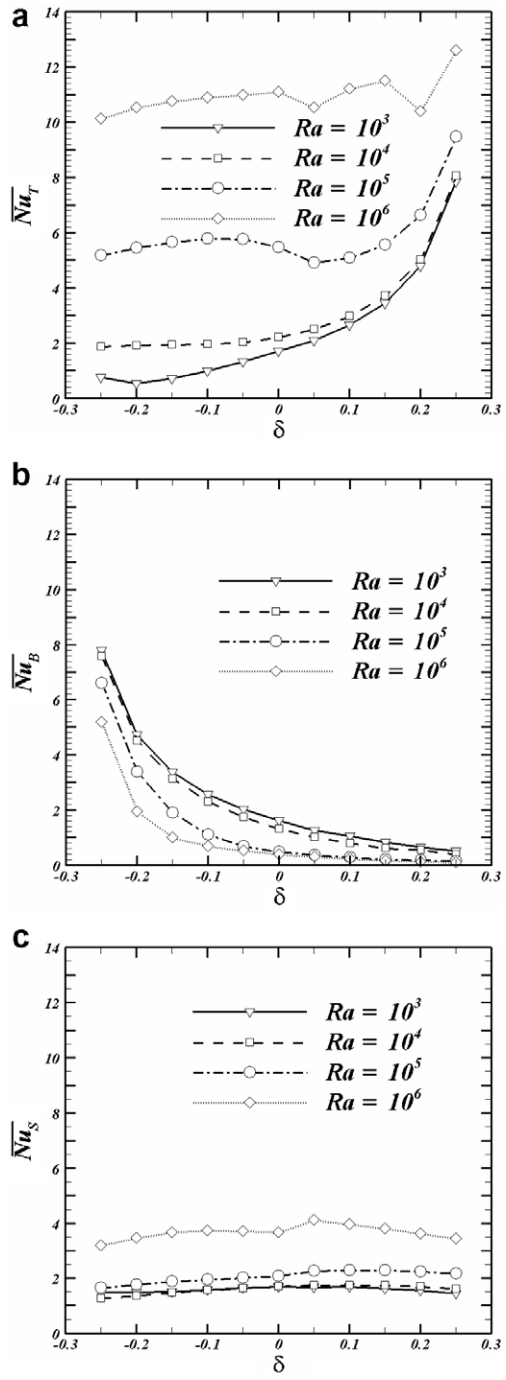

Fig. 13. Surface-averaged Nusselt number as a function of δ for four different Rayleigh number on each wall; (a) top wall, (b) bottom wall and (c) side wall.

inner cylinder and the top wall of the enclosure is smallest in the absence of the secondary and tertiary vortices.

Fig. 13b shows the surface-averaged Nusselt number at the bottom wall of the enclosure, $\overline{Nu}_B$, as a function of δ for different Rayleigh numbers. $\overline{Nu}_B$ decreases generally with increasing Rayleigh number due to the increasing effect of convection. When the distance between the inner cylinder and the bottom wall of the enclosure increases with increasing δ, $\overline{Nu}_B$ decreases due to the decreasing thermal gradient on the bottom wall. When $0 \leqslant \delta \leqslant 0.25$, $\overline{Nu}_B$ decreases slowly with increasing δ. However, when $-0.25 \leqslant \delta \leqslant 0$, $\overline{Nu}_B$ decreases very rapidly with increasing δ, showing the large dependence of $\overline{Nu}_B$ on δ in this region. The presence of the secondary and tertiary vortices on the upper surface of the inner cylinder has some influences on the distribution of isotherms and their corresponding variation of $\overline{Nu}_T$. However, the effect of the presence of the additional vortices on the bottom wall on the distribution of isotherms and their corresponding variation of $\overline{Nu}_B$ is very small.

Fig. 13c shows the surface-averaged Nusselt number at the side wall of the enclosure, $\overline{Nu}_S$, as a function of δ for different Rayleigh numbers. $\overline{Nu}_S$ also increases generally with increasing Rayleigh number due to the increasing effect of convection. However, the effect of δ on $\overline{Nu}_S$ is small whereas the effect of Ra on $\overline{Nu}_S$ is large, unlike the cases of $\overline{Nu}_T$ and $\overline{Nu}_B$.

Fig. 14 shows the total surfaces-averaged Nusselt number of the enclosure, $\overline{Nu}_{en}$, and the surface-averaged Nusselt number of the inner cylinder, $\overline{Nu}_C$, as a function of δ for different Rayleigh numbers. $\overline{Nu}_{en}$ represents the surface-averaged sum of $\overline{Nu}_T$, $\overline{Nu}_B$ and $\overline{Nu}_S$ shown in Fig. 13a–c.

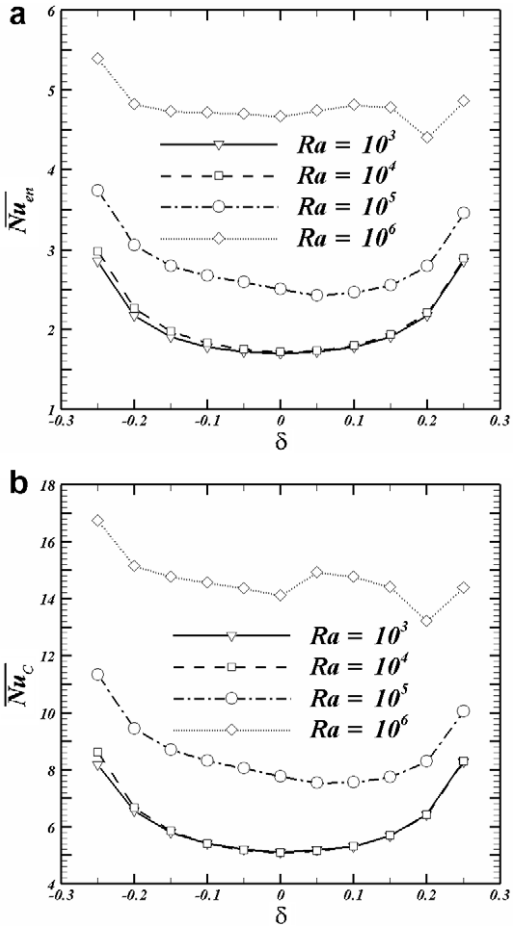

Fig. 14. Total surfaces-averaged Nusselt number of the enclosure, $\overline{Nu}_{en}$ and the surface-averaged Nusselt number, $\overline{Nu}_C$ of the inner cylinder along the δ for the different Rayleigh numbers.

When $Ra = 10^3$ and 10^4, $\overline{Nu}_{en}$ has a parabolic profile with a minimum value at $\delta = 0$. The value of $\overline{Nu}_{en}$ at $Ra = 10^4$ is almost the same as that at $Ra = 10^3$. However, when the Rayleigh number increases to 10^5, the symmetry of $\overline{Nu}_{en}$ is broken and $\overline{Nu}_{en}$ has a minimum value at $\delta = 0.05$, because of the presence of the secondary vortices formed on the upper surface of the inner cylinder owing to the rising thermal plumes. The value of $\overline{Nu}_{en}$ at $\delta = 0.25$ is smaller than that at $\delta = -0.25$, because the stagnant region at $\delta = 0.25$ becomes larger than that $\delta = -0.25$. When $-0.25 \leqslant \delta \leqslant 0$ at $Ra = 10^6$, $\overline{Nu}_{en}$ decreases with increasing δ, similar to the cases when $Ra = 10^3$, 10^4 and 10^5. However, when $0 \leqslant \delta \leqslant 0.25$ at $Ra = 10^6$, the variation of $\overline{Nu}_{en}$ according to the variation of δ is different from that when $Ra = 10^3$, 10^4 and 10^5, due to the combined effect of both the formation of the secondary and tertiary vortices and the distance between the inner cylinder and top and bottom walls of the enclosure. With increasing δ, $\overline{Nu}_{en}$ increases at $0 \leqslant \delta \leqslant 0.15$, decreases at $\delta = 0.2$ and increases again at $\delta = 0.25$. The pattern of the variation of $\overline{Nu}_{C}$ as a function of δ is generally similar to that of $\overline{Nu}_{en}$. However, the magnitude of $\overline{Nu}_{C}$ is larger than that of $\overline{Nu}_{en}$ for all different cylinder positions because the isotherms are formed more densely on the inner cylinder surface than that on the surfaces of the enclosure, as shown in Figs. 3–7.

4. Conclusions

The present study investigates numerically the characteristics of a two-dimensional natural convection problem in a cooled square enclosure with an inner heated circular cylinder. The immersed boundary method was implemented in a second-order accurate finite volume method to simulate the flow and heat transfer over an inner circular cylinder in the Cartesian coordinates. A detailed analysis for the distribution of streamlines, isotherms and Nusselt number was carried out to investigate the effect of the locations of the heated inner cylinder on the fluid flow and heat transfer in the cooled square enclosure for different Rayleigh numbers in the range of $10^3 \leqslant Ra \leqslant 10^6$.

For all Rayleigh numbers considered in the present study, the flow and thermal fields eventually reach the steady state with the symmetric shape about the vertical center line through the center of the inner circular cylinder. Thus the present problem has a two-fold symmetry about the vertical center line at $x = 0$.

At low Rayleigh numbers of 10^3 and 10^4, the bifurcation from the bi-cellular vortices to an uni-cellular vortex occurs when an inner cylinder is placed at a certain distance from the center of the enclosure. When $Ra = 10^5$ and 10^6, only an uni-cellular vortex is formed in the enclosure irrespective of the position of the inner cylinder. At these high Rayleigh numbers, the effect of the inner cylinder position on fluid flow and heat transfer is significant, especially in the upper half region. As a result, when $Ra = 10^5$, the secondary vortices due to the rising thermal plume from the inner cylinder are present on the upper surface of the inner cylinder. When the inner cylinder approaches to the top wall at $Ra = 10^6$, additional vortices are formed near the bottom wall in addition to the secondary and tertiary vortices formed near the upper surface of the inner cylinder, due to the stronger convective force with increasing Rayleigh number.

The presence of the secondary and tertiary vortices near the upper surface of the inner cylinder according to the variation of the inner cylinder position and Rayleigh number has big influences on the distribution of the local and surface-averaged Nusselt numbers. The location of the peak and the valley of the local Nusselt numbers along the surfaces of the inner cylinder and enclosure depends much on the location of the center of these vortices.

The variation of the total surface-averaged Nusselt number of the enclosure as a function of δ for different Rayleigh numbers is similar to the surface-averaged Nusselt numbers of the inner cylinder. When $Ra = 10^3$ and 10^4, $\overline{Nu}_{en}$ and $\overline{Nu}_{C}$ have a parabolic profile with a minimum value at $\delta = 0$ and show a symmetric shape around $\delta = 0$. When $Ra = 10^5$ and 10^6, the profiles of $\overline{Nu}_{en}$ and $\overline{Nu}_{C}$ are not symmetric due to the presence of the secondary vortices at $Ra = 10^5$ and tertiary vortices in addition to secondary vortices at $Ra = 10^6$ on the upper surface of the inner cylinder caused by the rising plume from the inner cylinder. The value of $\overline{Nu}_{C}$ is larger than that of $\overline{Nu}_{en}$, because the isotherms are formed more densely on the inner cylinder surface than that on the surfaces of the enclosure.

Acknowledgement

This works was partially supported by Brain Korea 21. Prof. Yoon thanks the Advanced Ship Engineering Research Center (ASERC) of Pusan National University for the financial support through the Korea Science and Engineering Foundation.

References

[1] M. Lacroix, Natural convection heat transfer around two heated horizontal cylinders inside a rectangular cavity cooled from above, Numer. Heat Transfer Part A 21 (1992) 37–54.
[2] N.K. Ghaddar, F. Thiele, Natural convection over a rotating cylindrical heat source in a rectangular enclosure, Numer. Heat Transfer Part A 26 (1994) 701–717.
[3] A.K. Saha, Unsteady free convection in a vertical channel with a built-in heated square cylinder, Numer. Heat Transfer Part A 38 (2000) 795–818.
[4] H. Ding, C. Shu, K.S. Yeo, Z.L. Lu, Simulation of a natural convection in eccentric annuli between a square outer cylinder and a circular inner cylinder using a local MQ–DQ method, Numer. Heat Transfer Part A 47 (2005) 291–313.
[5] M.Y. Ha, I.K. Kim, H.S. Yoon, S.S. Lee, Unsteady fluid flow and temperature fields in a horizontal enclosure with an adiabatic body, Phys. Fluids 14 (2002) 3189–3202.
[6] M.Y. Ha, I.K. Kim, H.S. Yoon, K.S. Yoon, J.R. Lee, S. Balachandar, H.H. Chun, Two-dimensional and unsteady natural convection in a horizontal enclosure with a square body, Numer. Heat Transfer Part A 41 (2002) 183–210.

[7] J.R. Lee, M.Y. Ha, A numerical study of natural convection in a horizontal enclosure with a conducting body, Int. J. Heat Mass Transfer 48 (2005) 3308–3318.
[8] J.R. Lee, M.Y. Ha, Numerical simulation of natural convection in horizontal enclosure with heat-generating conducting body, KSME. J 29 (2005) 441–452.
[9] J.R. Lee, M.Y. Ha, S. Balachandar, H.S. Yoon, S.S. Lee, Natural convection in a horizontal layer of fluid with a periodic array of square cylinders in the interior, Phys. Fluids 16 (2004) 1273–1286.
[10] J.M. Hyun, J.W. Lee, Numerical solutions for transient natural convection in a square cavity with different sidewall temperatures, Int. J. Heat Fluid Flow 10 (1989) 146–151.
[11] D. Misra, A. Sarkar, Finite element analysis of conjugate natural convection in a square enclosure with a conducting vertical wall, Comput. Methods Appl. Mech. Eng. 141 (1997) 205–219.
[12] J.L. Wright, H. Jin, K.G.T. Hollands, D. Naylor, Flow visualization of natural convection in a tall, air-filled vertical cavity, Int. J. Heat Mass Transfer 49 (2006) 889–904.
[13] G.D. McBain, Natural convection with unsaturated humid air in vertical cavities, Int. J. Heat Mass Transfer 40 (1997) 3005–3012.
[14] M. Jami, A. Mezrhab, M. Bouzidi, P. Lallemand, Lattice Boltzmann method applied to the laminar natural convection in an enclosure with a heat-generating cylinder conducting body, Int. J. Thermal Sci. 46 (2007) 38–47.
[15] M.Y. Ha, M.J. Jung, A numerical study on there-dimensional conjugate heat transfer of natural convection and conduction in a differentially heated cubic enclosure with a heat-generating cubic conducting body, Int. J. Heat Mass Transfer 43 (2000) 4229–4248.
[16] H. Asan, Natural convection in an annulus between two isothermal concentric square ducts, Int. Comm. Heat Mass Transfer 27 (2000) 367–376.
[17] A. Kumar De, A. Dalal, A numerical study of natural convection around a square, horizontal, heated cylinder placed in an enclosure, Int. J. Heat Mass Transfer 49 (2006) 4608–4623.
[18] N.K. Ghaddar, Natural convection heat transfer between a uniformly heated cylindrical element and its rectangular enclosure, Int. J. Heat Mass Transfer 35 (1992) 2327–2334.
[19] G. Cesini, M. Paroncini, G. Cortella, M. Manzan, Natural convection from a horizontal cylinder in a rectangular cavity, Int. J. Heat Mass Transfer 42 (1999) 1801–1811.
[20] F. Moukalled, S. Acharya, Natural convection in the annulus between concentric horizontal circular and square cylinders, J. Thermophys. Heat Transfer 10 (1996) 524–531.
[21] C. Shu, Y.D. Zhu, Efficient computation of natural convection in a concentric annulus between an outer square cylinder and an inner circular cylinder, Int. J. Numer. Meth. Fluids 38 (2002) 429–445.
[22] C. Shu, H. Xue, Y.D. Zhu, Numerical study of natural convection in an eccentric annulus between a square outer cylinder and a circular inner cylinder using DQ method, Int. J. Heat Mass Transfer 44 (2000) 3321–3333.
[23] J. Kim, P. Moin, Application of a fractional step method to incompressible Navier–Stokes equations, J. Comp. Phys. 59 (1985) 308–323.
[24] Y. Zang, R.L. Street, J.R. Koseff, A non-staggered grid, fractional step method for time-dependent incompressible Navier–Stokes equations in curvilinear coordinates, J. Comp. Phys. 114 (1994) 18–33.
[25] J. Kim, D. Kim, H. Choi, An immersed-boundary finite volume method for simulations of flow in complex geometries, J. Comp. Phys. 171 (2001) 132–150.
[26] J. Kim, H. Choi, An immersed-boundary finite-volume method for simulation of heat transfer in complex geometries, KSME Int. J. 18 (2004) 1026–1035.